Jpn. J. Appl. Phys. Vol. 40 (2001) pp. 2100–2104
Part 1, No. 3B, March 2001

A Double Quantum Dot as an Artificial Two-Level System

Wilfred G. van der WIEL[1], Toshimasa FUJISAWA[2], Seigo TARUCHA[2,3] and Leo P. KOUWENHOVEN[1]
[1]*Department of Applied Physics, DIMES, and ERATO Mesoscopic Correlation Project, Delft University of Technology, P.O. Box 5046, 2600 GA Delft, The Netherlands*
[2]*NTT Basic Research Laboratories, Atsugi-shi, Kanagawa 243-0198, Japan*
[3]*ERATO Mesoscopic Correlation Project, University of Tokyo, Bunkyo-ku, Tokyo 113-0033, Japan*

(Received September 1, 2000; accepted for publication November 27, 2000)

We study an artificial two-level system formed by a double quantum dot. Microwave spectroscopy experiments are discussed, in which we show that the inter-dot coupling can be tuned from ionic-like to covalent-like. The current through the double dot system is dependent on the applied microwave power and, in case of strong inter-dot coupling, the separation between the bonding and anti-bonding state is power dependent as well. We measure the elastic and inelastic transitions between the two levels. The inelastic transition rates are well described by Bose-Einstein statistics. Acoustic phonons are the most effectively coupled bosons in the solid-state environment of the two-level system.

KEYWORDS: two-level system, quantum dots, photon-assisted tunneling, spontaneous emission, mesoscopic physics

1. Introduction

In principle, any quantum two-level system can be applied to form a quantum bit, or qubit, the basic building block for quantum logic. One of the physical systems in which an artificial two-level system can be realized, is a double quantum dot, a system of two quantum dots coupled to each other. Quantum dots are often referred to as artificial atoms, because of their analogies with real atoms[1)] and hence the name "artificial molecule" for a double dot system. Our quantum dots are man-made "droplets" of charge in a semiconductor heterostructure, containing a variable number of electrons.[2)] Their size is typically $\sim$ 100 nm and their shape and interactions can be precisely controlled through nanofabrication technology. This controllability allows us to study the manipulation of quantum states for future quantum logic gates. Here, we present microwave (0–50 GHz) spectroscopy experiments on double quantum dots for different coupling and microwave power regimes. For weakly coupled dots we show in §2 how the height of the main resonance and the photon-assisted current peaks (absorption and emission) are affected by high-power microwave irradiation. In §3 it is discussed how a high-power microwave influences the energy splitting between the bonding and anti-bonding states in the double dot. Section 4 deals with the spontaneous emission spectrum in double quantum dot devices. Spontaneous emission processes can form a source of decoherence and make the application as a qubit difficult.

2. Weakly Coupled Dots

If the inter-dot coupling is weak, electrons are strongly localized on the individual dots. The double dot is tuned in the regime such that only one level in each dot contributes to electron transport.[3)] The gate voltages are used to surmount the single-electron charging energy and to align a discrete energy level in the left dot with a discrete energy level in the right dot.[2)] Then, it is energetically allowed for an electron to tunnel between the dots. A current can flow when the two energy levels are aligned within the bias voltage window, defined by the electrochemical potentials of the left and right lead. Note that energy is also conserved when photons of energy hf, which match the energy difference between the states of the two dots, are absorbed from the microwave field (see upper inset to Fig. 1(b)). The possible tunnel processes are schematically depicted at the top of Fig. 1(a). The lower inset to Fig. 1(b) shows a scanning electron microscope (SEM) photograph of the double dot device in which the source and drain regions and the double dot are indicated schematically.[4)] The resonance in the lowest trace in Fig. 1(a) is due to an alignment of discrete energy levels. The other traces are measured while applying a microwave signal. The satellite resonances are due to photon assisted tunneling (PAT) processes which involve the emission (left satellite) or absorption (right satellite) of a microwave photon.[5)] An ac voltage drop $V = V_{\rm ac}\cos(2\pi f t)$ ($V_{\rm ac}$ and f are the microwave amplitude and frequency, respectively) across a tunnel barrier modifies the tunnel rate through the barrier as

$$\Gamma^*(E) = \sum_{n=-\infty}^{\infty} \mathrm{J}_{\rm n}^2(\alpha)\Gamma(E + nhf). \qquad (1)$$

Here $\Gamma^*(E)$ and $\Gamma(E)$ are the tunnel rates at energy E with and without an ac voltage, respectively. $\mathrm{J}_{\rm n}^2(\alpha)$ is the square of the nth order Bessel function evaluated at $\alpha = eV_{\rm ac}/hf$, which describes the probability that an electron absorbs or emits n photons of energy hf. The squared Bessel functions for $n = 0$, 1, 2 are given in Fig. 1(c). The inset schematically shows the first two photon side bands developed in the presence of a microwave field.

As the power is increased, satellite peaks appear corresponding to the absorption of multiple photons, which are observed up to $n = 11$.[3)] A high power microwave field strongly perturbs tunneling. This is reflected by the non-linear dependence of the peak heights on microwave power. In Fig. 1(d) the peak heights of the main peak and the first two photon satellite peaks are shown, which agree well with the expected squared Bessel function behavior as shown in Fig. 1(c).

Figure 1(b) shows that the energy separation of the satellite peaks from the main peak, ΔE, depends linearly on frequency between 1 and 50 GHz. As we will discuss in §3, this linearity implies that the tunnel coupling is negligible. The electrons are localized on the individual dots and they have an ionic bonding. The line proportional to $2hf$ is taken from data at higher microwave powers where electrons absorb or emit two photons during tunneling.

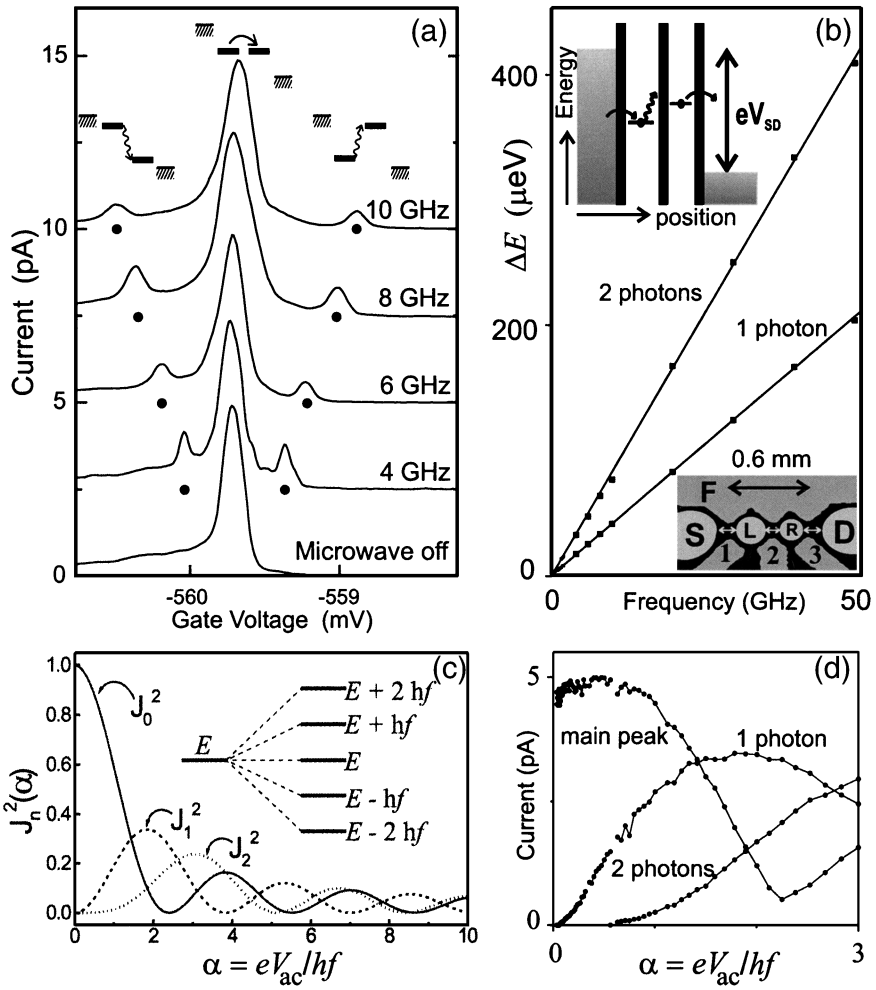

Fig. 1. Weakly coupled double quantum dot in the low and high microwave power regime. (a) The upper schematic pictures illustrate three situations of the energy state in the left dot relative to the state in the right dot. The hatched lines denote the Fermi seas in the leads. The bottom curve shows the current as a function of the voltage on gate 1 (see lower inset to Fig. 1(b)) for source-drain voltage, $V_{SD} = 500\,\mu$V without applying microwaves. A single resonance occurs when two states line up. The other curves, which have been offset for clarity, show the current when microwaves with frequency f from 4 to 10 GHz are applied. Now, two additional satellite resonances occur when the two states are exactly a photon energy apart. The corresponding photon-assisted tunneling processes are illustrated in the upper diagrams. (b) Distance between main resonance and first two satellites as a function of the applied frequency from 1 to 50 GHz. The distance is transferred to energy through $\Delta E = \kappa \Delta V_g$ where κ is the appropriate capacitance ratio for our device that converts gate voltage to energy.[2] The agreement between data points and the two solid lines, which have slopes of h and $2h$, demonstrates that we observe the expected linear frequency dependence of the one and two photon processes. Upper inset, diagram of the electron energies in the double dot for the case that an electron needs to absorb a photon in order to contribute to the current. Lower inset, SEM micrograph of double quantum dot used for the presented measurements.[4] The left (L) and right (R) dot, the source (S) and drain (D) contacts, and the gate electrodes (1, 2, 3, F) are indicated. (c) Squared Bessel functions of the first kind, $J_n^2(\alpha)$, for $n = 0$, 1, 2. The inset schematically shows the development of sidebands of the original energy as a consequence of the microwave field. A positive or negative n corresponds to the absorption or emission, respectively, of n photons during the tunnel process. Elastic tunneling corresponds to $n = 0$. (d) Height of the main current peak and the first two satellite peaks as function of normalized microwave power. The experimental height dependence agrees with the expected squared Bessel function behavior as shown in (c).

3. Strongly Coupled Dots

The experiments for strong inter-dot coupling were performed on a second type of double-dot sample (see inset to Fig. 3(a)).[6] To single out the current only due to microwaves we operate the device as an electron pump driven by photons[7,8] (see the diagrams in Fig. 2(a)). When the two dots are strongly coupled, a bonding and anti-bonding eigenstate is formed. The energy separation between the bonding and anti-bonding eigenstates, ΔE^*, is given by $\Delta E^* = \sqrt{\{\Delta E\}^2 + \{2J_0(\alpha)T\}^2}$, where ΔE is the uncoupled energy splitting ($\Delta E = E_L - E_R$) and T is the tunnel coupling between the two dots. When the sample is irradiated, an excitation may result as illustrated in Fig. 2(a). A non-zero current indicates that an electron is excited from the bonding to the anti-bonding state, thereby fulfilling the condition $hf = \Delta E^*$, or conversely

$$\Delta E = \sqrt{\{hf\}^2 - \{2J_0(\alpha)T\}^2}. \quad (2)$$

In Fig. 2(b) the so called stability diagram of the double dot is given, clearly showing the energy regions of constant charge and the signatures of PAT. The coupling between the dots can be decreased by changing the gate voltage on the center gate to more negative values or by applying a magnetic field perpendicular to the sample.

In Fig. 3(a) we have plotted the energy spacing ΔE at

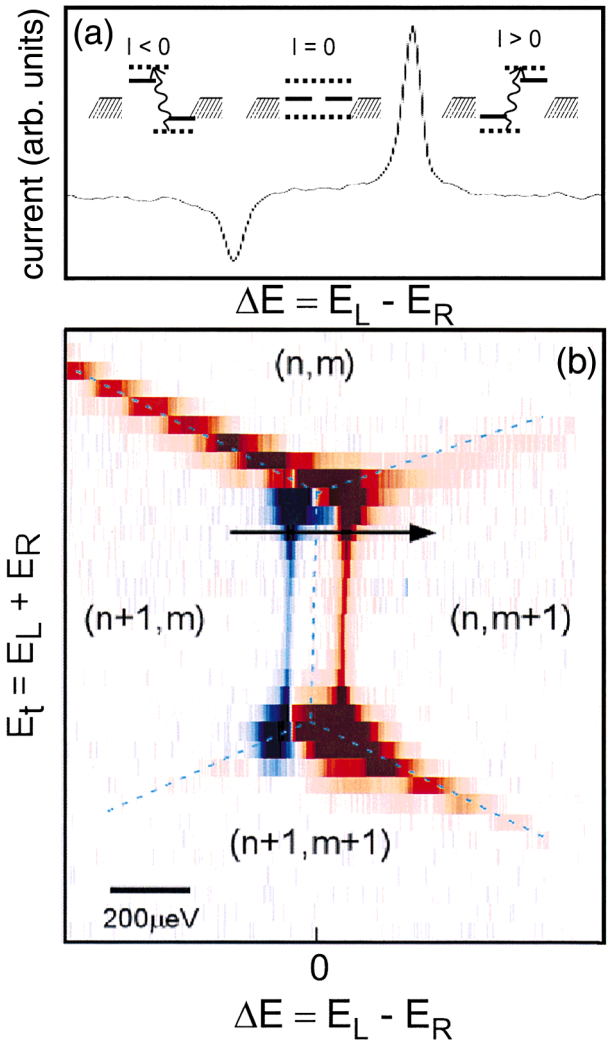

Fig. 2. Strongly coupled double dot in the low-power regime. (a) Current through the double as function of the energy difference between the level in the left and the right dot. The current trace is taken from the stability diagram in (b) at the position indicated by the arrow. In the energy diagrams the solid lines depict the energy states E_L and E_R in the two dots for the case that the coupling is weak and that their energy difference is simply $\Delta E = E_L - E_R$. When the dots are strongly coupled, the states delocalize over both dots thereby forming a bonding and an anti-bonding state. These are indicated by two dotted lines. Their energy difference is $\Delta E^* = \sqrt{\{\Delta E\}^2 + \{2J_0(\alpha)T\}^2}$. Electrons are transferred from the bonding to the anti-bonding state when $\Delta E^* = hf$. In the first diagram $E_L > E_R$, which results in electron pumping from right to left corresponding to the negative current peak. In the second diagram the whole system is symmetric $E_L = E_R$ and consequently the net electron flow must be zero. In the third diagram $E_L < E_R$, which gives rise to pumping from left to right and a positive current peak. (b) Color scale plot of the current through the double dot versus the energy level difference, ΔE, and the total energy, E_t. The bias voltage is 6 μV and the applied microwave frequency is 16 GHz. Red (blue) corresponds with positive (negative) current. The dashed lines divide the stability diagram in 4 regions in which the respective electron number in the left dot, n, and right dot, m, are indicated. At the position where 3 dashed lines intersect, the triple points, two levels align at the Fermi level. In between the two triple points clear features of photon-assisted tunneling are seen. The black arrow indicates the position of the trace shown in (a).

which the pumping current is at a maximum, as a function of frequency. The microwave power is kept as low as possible in order to meet the condition $eV_{ac} \ll hf$. In that case $J_0^2(\alpha) \approx 1$ and the relation

$$\Delta E = \sqrt{\{hf\}^2 - \{2T\}^2}, \tag{3}$$

is expected to be valid. Different labels correspond to different center gate voltage settings and magnetic fields. The solid lines are fits of eq. (3) to the measured data. It follows that the coupling $2T$ has been tuned from 11 to 60 μeV. The good agreement with eq. (3) demonstrates the control over the formation of a covalent bonding between the two dots and that the condition $eV_{ac} \ll hf$ has been satisfied.

We now discuss the case $eV_{ac} \gtrsim hf$. As can be seen in Fig. 1(c), $J_0^2(\alpha)$ deviates from 1 in this case and cannot be neglected as before.[9] Below we discuss for a coupling of 60 μeV and a microwave frequency of 16 GHz, as indicated by the circle in Fig. 3(a). Similar results have been obtained for other couplings and microwave frequencies. The inset to Fig. 3(b) shows the measured PAT current as a function of ΔE for different powers. The absolute value of the microwave power at the position of the double quantum dot is unknown. Therefore, we use a relative microwave power scale, which is expressed in terms of the attenuation of the microwave source signal in units dB. The positions of the PAT peaks at the lowest power are indicated with two dashed lines. Increasing the microwave power from the lowest value, the PAT peak separation becomes larger, which is in agreement with eq. (2). For higher powers, multiple-photon processes can take place, which result in extra current peaks. Additional structure in the high power current measurements can also be caused by photon assisted pumping,[10] which is due to an asymmetric ac voltage drop across the double dot. Figure 3(b) shows half the PAT peak separation energy as function of the relative microwave power. The solid line is a fit with eq. (2), $f = 16$ GHz, $2T = 60$ μeV. Because of the relative power scale, the fitting curve has been adjusted horizontally to give the best fit. The microwave power effectively reduces the coupling between the dots. This is illustrated by the vertical dotted line in Fig. 3(a) at $f = 16$ GHz. At -33 dB the energy separation equals hf, which implies that the effective coupling is zero. This means $J_0^2(\alpha)$ has its first zero and $\alpha = eV_{ac}/hf = 2.4$ and hence $V_{ac} = 0.16$ mV. This provides an estimate for the absolute power applied to the device.

4. Spontaneous Emission Spectrum

Coupling a quantum two-level system to a bosonic environment gives rise to inelastic processes, which reduce the coherence of the system. Even at the lowest temperatures spontaneous emission (emission stimulated by vacuum fluctuations) can take place. For higher temperatures also absorption of bosons is possible. We use the same double dot device as shown in Fig. 3(a) in the weakly coupled regime for the study of the spontaneous emission spectrum of a controllable two-level system.[11] A double quantum dot has a tunable energy selectivity to its environment, since the system can emit and absorb energy quanta equal to the energy spacing of the two levels.

A typical current spectrum versus $\Delta E = E_L - E_R$ at our lowest lattice temperature $T = 23$ mK is shown in Fig. 4(a) for both a positive and negative source drain voltage. The gate voltages V_{G1} and V_{G2} are swept simultaneously such that the respective energies are like those illustrated in the diagrams in Fig. 4(a). $\Delta E = 0$ occurs in the middle between the Fermi

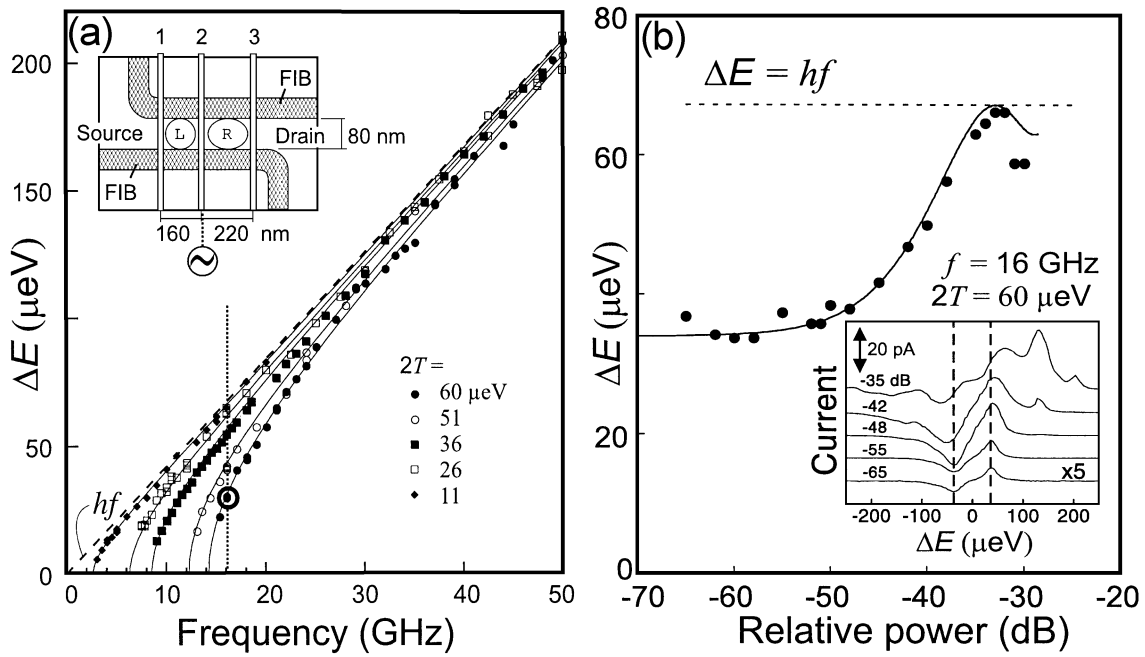

Fig. 3. (a) Half the spacing in gate voltage between the positive and negative satellite peaks as a function of frequency. The microwave power is kept as low as possible in order to meet the condition $eV_{ac} \ll hf$. In that case $J_0^2(\alpha) \approx 1$ and the relation $\Delta E = \sqrt{\{hf\}^2 - \{2T\}^2}$ is expected to be valid. Gate voltage spacing has been transferred to energy difference ΔE (see also figure caption 1(b)). Different curves correspond to different coupling constants T. Solid lines are theoretical fits to $\Delta E = \sqrt{\{hf\}^2 - \{2T\}^2}$. In the limit of weak-coupling, this reduces to $\Delta E = hf$, which is indicated by the dashed line. The resulting values for $2T$ are given in the figure. The coupling is varied by applying different voltages to the center gate (2) or by changing the magnetic field (◆ $B = 3.3$ T; ■ $B = 2.2$ T; other curves $B = 0$ T). The upper left inset shows a diagram of the sample.[6] A narrow channel is defined by locally depleting the 2DEG using focussed ion beam (FIB) implantation. Applying negative voltages to the three gates (1, 2, 3) that cross the channel then forms two dots. Microwaves are capacitively coupled to gate 2. The circle marks a coupling of 60 μeV and frequency of 16 GHz (dotted line), which are the conditions used for the high power results shown in (b). (b) Strongly coupled double dot ($2T = 60\,\mu$eV) in the high microwave power regime for $f = 16$ GHz. The inset shows the measured PAT current as a function of ΔE for different powers. We use a relative microwave power scale, which is expressed in terms of the attenuation of the microwave source signal in units dB. The positions of the PAT peaks at the lowest power are indicated with two dashed lines. Increasing the microwave power from the lowest value, the PAT peak separation becomes larger. For higher powers, multiple photon processes can take place, which result in extra current peaks. Additional structure in the high power current measurements can also be caused by photon assisted pumping,[10] which is due to an asymmetric ac voltage drop across the double dot. In the main part, half the PAT peak separation energy as function of the relative microwave power is shown. The solid line is a fit to $\Delta E = \sqrt{\{hf\}^2 - \{2J_0(\alpha)T\}^2}$, $f = 16$ GHz, $2T = 60\,\mu$eV. Because of the relative power scale, the fitting curve has been adjusted horizontally to obtain the best fit.

energies of source and drain and $|\Delta E| = eV_{SD}$ corresponds to having the states E_L and E_R aligned to one of the Fermi energies. The inelastic current appears for positive ΔE when $V_{SD} > 0$ and for negative ΔE when $V_{SD} < 0$, where emission occurs.

For a quantitative analysis, we decompose the current into a symmetric, elastic part $I_{el}(\Delta E) = I_{el}(-\Delta E)$ (dashed curve) and the remaining asymmetric, inelastic part $I_{inel}(\Delta E > 0)$ (dotted-dashed curve) as shown in the inset to Fig. 4(b). The elastic current should have a Lorentzian line shape.[4,5] The inelastic process should be sequential tunneling of the three barriers, which yields

$$I_{inel} = e(\Gamma_L^{-1} + \Gamma_{inel}^{-1}(\Delta E) + \Gamma_R^{-1}), \tag{4}$$

where Γ_L and Γ_R are the tunneling rates for the left and right barriers. When Γ_L and Γ_R are larger than the inelastic tunneling rate, Γ_{inel}, the current becomes $I_{inel}(\Delta E) = e\Gamma_{inel}$.

The temperature dependence of the inelastic current is shown in Fig. 4(b). A higher temperature T enhances the inelastic current on both the emission and the absorption side. In the following analysis, we assume boson statistics for the degree of freedom in the environment. The average occupation number $\langle n \rangle$ of environmental modes is given by the Bose-Einstein distribution function: $\langle n \rangle = 1/(e^{\Delta E/kT} - 1)$. The rates for absorption, W_a, and emission, W_e, can be expressed very generally by $W_a = B_a\rho$ and $W_e = A + B_e\rho$, where the Einstein coefficients stand for spontaneous emission (A), stimulated emission (B_e) and absorption (B_a), and ρ is the energy density.[12] From the Einstein relations, $B_a = B_e = A\langle n \rangle/\rho$, we obtain

$$\Gamma_{inel}(\Delta E < 0) = W_a(\Delta E) = \langle n \rangle A(-\Delta E)$$
$$\Gamma_{inel}(\Delta E > 0) = W_e(\Delta E) = (\langle n \rangle + 1)A(-\Delta E). \tag{5}$$

The normalized rates W_e/A and W_a/A are plotted versus $kT/|\Delta E|$ for various ΔE and T in Fig. 4(c). The measured data follow the $\langle n \rangle$ and $\langle n \rangle + 1$ curves without any fitting parameter.

The energy dependence of the inelastic current suggests that the bosonic environment coupled to the double dot is formed by acoustic phonons.[11] In solid-state systems the electron-acoustic phonon ineteraction is strong. The typical emission rate in a single quantum dot at zero temperature can be 10^8–10^{10} s^{-1}, due to deformation or piezoelectric interaction.[13] Since the wave functions in a double dot are spatially separated, the spontaneous emission rate is lower, but still

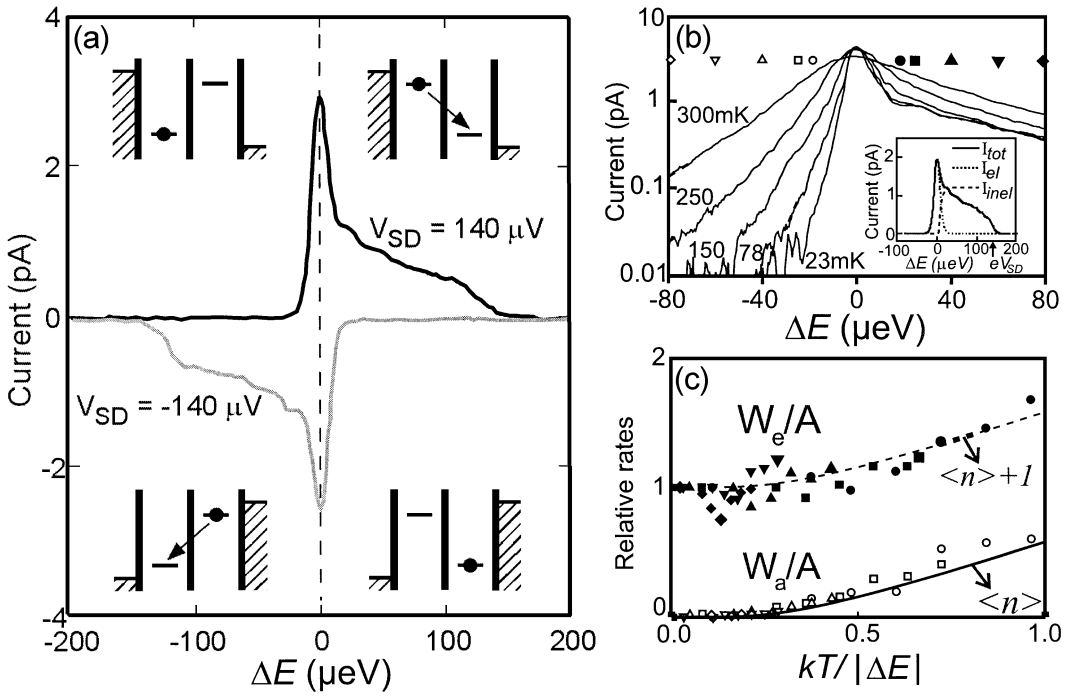

Fig. 4. Spontaneous emission spectrum in double dots. (a) Current versus $\Delta E = E_L - E_R$ for $V_{SD} = 140\,\mu$V and $V_{SD} = -140\,\mu$V at 23 mK. The current is measured while sweeping V_{G1} and V_{G2} (see inset to Fig. 3(a)) simultaneously in opposite directions such that we change the energy difference ΔE. For $\Delta E = 0$ a resonant elastic current peak is measured. The diagrams show the position of the Fermi levels and discrete energy levels E_L and E_R in the four quadrants of the figure. Inelastic current is only measured in the cases that (spontaneous) emission can take place. (b) Current versus ΔE for $T = 23$ to 300 mK with $V_{SD} = 140\,\mu$V. Inelastic current is observed at the emission side ($\Delta E > 0$) and for higher temperatures also at the absorption side ($\Delta E < 0$). (c) The absorption rate W_a (open symbols) and emission rate W_e (closed symbols) normalized by the spontaneous emission rate A versus $kT/|\Delta E|$. Circles, squares, upper and lower triangles, and diamonds are taken at $|\Delta E| = 18$, 24, 40, 60, and 80 μeV, respectively (see also symbols in (b)). The solid line indicates the Bose-Einstein distribution, $\langle n \rangle$, whereas the dashed line shows $\langle n \rangle + 1$.

high enough to contribute an inelastic current of a few pA. We expect that the interaction with phonons can be controlled in phonon cavities, analogous to what is often realized in photon cavities.

5. Conclusions

Double quantum dot devices form controllable two-level systems. Microwave spectroscopy has been used to demonstrate the tunability of the inter-dot coupling. The solid state environment gives a significant contribution to inelastic processes. The inelastic transition rates are well described by Bose-Einstein statistics, where acoustic phonons are the main contributors.

Acknowledgments

We thank T. H. Oosterkamp, K. Ishibashi, R. Aguado, R. M. Schouten, Yu. V. Nazarov, T. H. Stoof, F. R. E. Mallens, S. F. Godijn, N. C. van der Vaart, S. M. Cronenwett, P. Hadley, C. J. P. M. Harmans, K. K. Likarev and J. E. Mooij for experimental help and useful discussions. This work was supported by the Dutch Organization for Research on Matter (FOM) and by the EU via a TMR network. L. P. K. was supported by the Dutch Royal Academy of Arts and Sciences (KNAW).

1) R. Ashoori: Nature **379** (1996) 413.
2) L. P. Kouwenhoven, C. M. Marcus, P. L. McEuen, S. Tarucha, R. M. Westervelt and N. S. Wingreen: *Electron transport* in *quantum dots in Mesoscopic Electron Transport*, eds. L. Sohn *et al.*, (Kluwer Series E, 1997) p. 105.
3) T. H. Oosterkamp, T. Fujisawa, W. G. van der Wiel, K. Ishibashi, R. V. Hijman, S. Tarucha and L. P. Kouwenhoven: Nature **395** (1998) 873.
4) N. C. van der Vaart, S. F. Godijn, Yu. V. Nazarov, C. J. P. M. Harmans, J. E. Mooij, L. W. Molenkamp and C. T. Foxon: Phys. Rev. Lett. **74** (1995) 4702.
5) T. H. Stoof and Yu. V. Nazarov: Phys. Rev. B **53** (1996) 1050.
6) T. Fujisawa and S. Tarucha: Superlatt. Microstruct. **21** (1997) 247.
7) C. A. Stafford and N. S. Wingreen: Phys. Rev. Lett. **76** (1996) 1916.
8) Ph. Brune, C. Bruder and H. Schoeller: Physica E **1** (1997) 216.
9) W. G. van der Wiel, T. Fujisawa, T. H. Oosterkamp and L. P. Kouwenhoven: Physica B **272/1-4** (1999) 31.
10) T. H. Oosterkamp, W. G. van der Wiel, S. de Franceschi, C. J. P. M. Harmans and L. P. Kouwenhoven: cond-mat/9904359 (1999).
11) T. Fujisawa, T. H. Oosterkamp, W. G. van der Wiel, B. W. Broer, R. Aguado, S. Tarucha and L. P. Kouwenhoven: Science **282** (1998) 932.
12) P. W. Milonni: The Quantum Vacuum, an Introduction to quantum electrodynamics (Academic Press, San Diego, 1994).
13) U. Bockelmann: Phys. Rev. B **50** (1994) 17271.